Sequential Side-Chain Residue Motions Transform the Binary into the Ternary State of DNA Polymerase λ

Meredith C. Foley, Karunesh Arora, and Tamar Schlick
Department of Chemistry and Courant Institute of Mathematical Sciences, New York University, New York, New York

ABSTRACT The nature of conformational transitions in DNA polymerase λ (pol λ), a low-fidelity DNA repair enzyme in the X-family that fills short nucleotide gaps, is investigated. Specifically, to determine whether pol λ has an induced-fit mechanism and open-to-closed transition before chemistry, we analyze a series of molecular dynamics simulations from both the binary and ternary states before chemistry, with and without the incoming nucleotide, with and without the catalytic Mg^{2+} ion in the active site, and with alterations in active site residues Ile^{492} and Arg^{517}. Though flips occurred for several side-chain residues (Ile^{492}, Tyr^{505}, Phe^{506}) in the active site toward the binary (inactive) conformation and partial DNA motion toward the binary position occurred without the incoming nucleotide, large-scale subdomain motions were not observed in any trajectory from the ternary complex regardless of the presence of the catalytic ion. Simulations from the binary state with incoming nucleotide exhibit more thumb subdomain motion, particularly in the loop containing β-strand 8 in the thumb, but closing occurred only in the Ile^{492}Ala mutant trajectory started from the binary state with incoming nucleotide and both ions. Further connections between active site residues and the DNA position are also revealed through our Ile^{492}Ala and Arg^{517}Ala mutant studies. Our combined studies suggest that while pol λ does not demonstrate large-scale subdomain movements as DNA polymerase β (pol β), significant DNA motion exists, and there are sequential subtle side chain and other motions—associated with Arg^{514}, Arg^{517}, Ile^{492}, Phe^{506}, Tyr^{505}, the DNA, and again Arg^{514} and Arg^{517}—all coupled to active site divalent ions and the DNA motion. Collectively, these motions transform pol λ to the chemistry-competent state. Significantly, analogs of these residues in pol β (Lys^{280}, Arg^{283}, Arg^{258}, Phe^{272}, and Tyr^{271}, respectively) have demonstrated roles in determining enzyme efficiency and fidelity. As proposed for pol β, motions of these residues may serve as gate-keepers by controlling the evolution of the reaction pathway before the chemical reaction.

INTRODUCTION

DNA Polymerase λ (pol λ), a member of the DNA polymerase-X family, which also includes DNA polymerase β (pol β) and African Swine Fever Virus DNA polymerase X (pol X), likely participates in repairing small damaged areas of DNA via the base excision repair mechanism and/or nonhomologous end joining pathway (1). Pol λ has no proofreading ability since it lacks 3′ → 5′ exonuclease activity (2). Experimental studies reveal that the polymerase activity of pol λ is less accurate than pol β and differs from other polymerases in generating far more frameshift errors than base substitution errors (1,3). The fidelity of pol λ has been determined to be in the range of 10^{-4}–10^{-5} (4).

Like other polymerases, pol λ consists of the characteristic polymerization domain of fingers, palm, and thumb (5), as well as an 8-kDa domain also found in pol β; pol λ also has an N-terminal BRCT domain (6,7) and a serine-proline rich linker region connecting the BRCT and 8-kDa domains. The 8-kDa domain of pol λ, like that of pol β, possesses 5′-deoxyribose-5-phosphate lyase activity (8).

Based on extensive kinetic, structural, and computational studies of various DNA polymerases (9–28), a common nucleotide insertion pathway has been proposed for a number of polymerases which undergo transitions between open and closed forms: after DNA binding, the DNA polymerase incorporates a 2′-deoxyribonucleoside 5′-triphosphate (dNTP) to form an open substrate complex. This complex may undergo a conformational change to align the catalytic groups and form a closed ternary complex. After this alignment, the nucleotidyl transfer reaction occurs: the 3′-OH of the primer strand attacks the P_α of the incoming dNTP to extend the primer strand and form the ternary product complex; this complex then undergoes a conformational change leading to the open enzyme form. This transition is followed by the dissociation of pyrophosphate, after which the DNA synthesis/repair cycle can begin again.

The large-scale subdomain conformational transition from an open to closed state is believed to be a key factor in determining DNA synthesis fidelity (29), while lack of large scale motions may be connected with low fidelity (30). Binding of the correct nucleotide is thought to induce the first conformational change whereas binding of an incorrect nucleotide may alter or inhibit this conformational transition. The induced-fit mechanism was thus proposed to explain the polymerase fidelity in the selection of the correct dNTP (31). Earlier dynamics simulations of pol β/DNA complexes with the enzyme's active site occupied by either the correct incoming basepair or no substrate have supported such a mechanism. These simulations have delineated the structural

Submitted June 23, 2006, and accepted for publication August 1, 2006.

Address reprint requests to Tamar Schlick, Tel.: 212-998-3116; E-mail: schlick@nyu.edu.

Karunesh Arora's present address is Dept. of Molecular Biology, The Scripps Research Institute, 10550 North Torrey Pines Road, La Jolla, CA 92037.

0006-3495/06/11/3182/14 $2.00

doi: 10.1529/biophysj.106.092080

and dynamic changes that occur before the nucleotidyl transfer reaction (25).

Recently, structures of pol λ complexes illustrating three distinct steps in the catalytic pathway for single-nucleotide gap filling have been resolved (32). The first complex is a 2.3 Å structure of a binary complex with single-nucleotide gapped DNA (PDB entry 1XSL). The second is a 1.95 Å ternary complex with 2′,3′-dideoxythymidine triphosphate (ddTTP) (PDB entry 1XSN) showing the enzyme-substrate complex in a state before chemistry. The third is a 2.2 Å structure of a ternary complex with nicked DNA and pyrophosphate (PDB entry 1XSP), reflecting the state after chemistry before the product is released (32).

A close examination of these structures reveals two possible key movements during the transition from the binary to the ternary state before the chemical reaction. The first motion consists of a shift in a loop containing β-strand 8 in the thumb coupled to a shift in the positions of β-strands 3 and 4 of the palm (32,33), as depicted in Fig. 1 *a*. These movements lead to a second rearrangement that repositions the DNA template strand with an ~5 Å shift, as shown in Fig. 1 *b*. This motion also repositions the templating base at the gap into a more favorable catalytic position, allowing it to base-pair with an incoming dNTP.

The above conformational motions in the transition from the binary to the ternary state of pol λ are minor compared to the large subdomain movements from an open to closed form already ascertained in the pol-β catalytic cycle (31,25). Since pol λ may remain closed even without the correct substrate (32,33), it is hypothesized that a large scale open-to-closed subdomain conformational transition is not required for pol λ's catalytic cycle (32,33). Indeed, x-ray crystal structures of another X-family DNA polymerase, murine terminal deoxynucleotidyltransferase, suggest no significant open-to-closed transformation (34). To determine what conformational transitions are involved in the catalytic cycle of pol λ and whether or not pol λ follows the induced-fit hypothesis, we perform a series of dynamics simulations from the binary and ternary states before chemistry with and without the incoming nucleotide.

We also explore the roles of both catalytic and nucleotide-binding Mg^{2+} ion positions in these simulations based upon pol-β data. Indeed, it is known that these ions affect subdomain conformational transitions before the nucleotidyl transfer reaction (25,26,28,35). Specifically, comprehensive structural, kinetic, and computational investigations of several polymerases (28,35) indicate that Mg^{2+} ions play an important role in stabilizing the closed active site conformation and attaining a three-dimensional geometry consistent with a two-metal-ion nucleotidyl transfer mechanism after the correct nucleotide binds (36). However, no catalytic Mg^{2+} ion has been observed in the ternary crystal structure of pol λ. To examine the role of the catalytic Mg^{2+} ion in assembling the active site in pol λ and determine its effect on conformational transitions, we perform simulations from both the binary and ternary states in the presence of the incoming nucleotide with and without the catalytic Mg^{2+} ion.

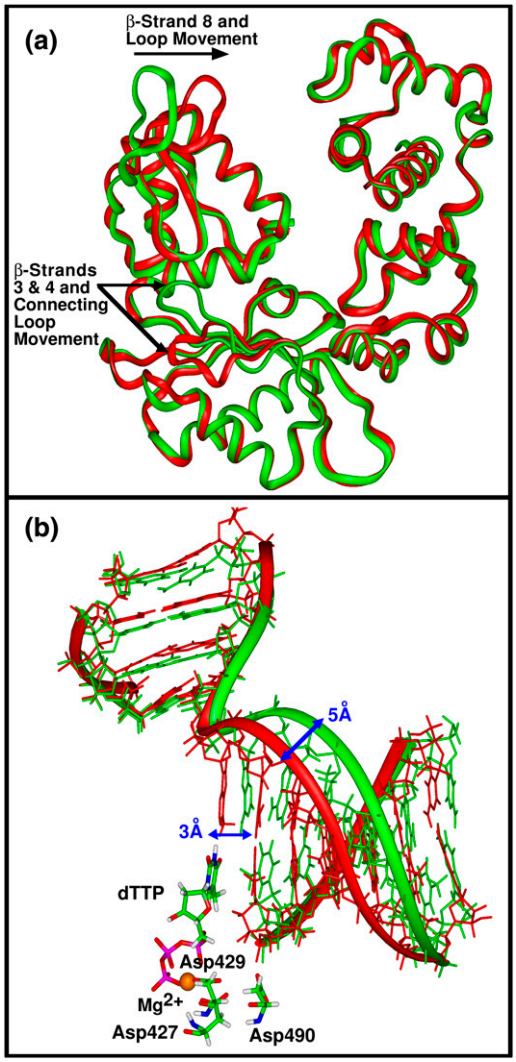

FIGURE 1 X-ray crystal binary (PDB entry 1XSL, *green*) and ternary (PDB entry 1XSN, *red*) pol λ/DNA complexes. (*a*) Superimposed C_α trace of x-ray crystal binary and ternary pol-λ complexes. Differences between the x-ray crystal structures in the thumb and palm subdomains are shown by the arrows. (*b*) Position of the DNA template strand and templating base at the gap in the x-ray crystal binary and ternary structures of pol λ. The incoming nucleotide (dTTP) and active-site residues Asp^{427}, Asp^{429}, and Asp^{490} of the ternary x-ray crystal structure are also shown. Key distances between the crystal binary and ternary states are provided and hydrogens are omitted from the DNA for clarity.

We emphasize, however, that force fields such as CHARMM and others are subject to many well-recognized limitations since they are described by empirical functions parameterized to match experimental data as closely as possible. For example, the energetics of divalent ions like Mg^{2+} are considered in the van der Waals (described by the phenomenological Lennard-Jones potential) and Coulombic interactions (37–40). Thus, while data generated for divalent ions with these force fields are generally useful and informative,

ligand/ion distances may be shorter than those observed in high resolution x-ray crystal structures. Clearly, caution is warranted when examining active-site geometries produced in molecular dynamics simulations. Because our study focuses on general trends in Mg^{2+} ion coordination and the long-range effects of the ions on subdomain motions and residue rearrangements, as well as involves systematic comparisons of the trends among closely-related systems, the above limitations of divalent ion representation are acceptable.

In addition to examining the transitions and the role of ions in the active site, we also investigate the roles of active-site pol λ residues Ile^{492} and Arg^{517} through mutant simulations. These two residues, Ile^{492} and Arg^{517}, are analogous to pol-β residues Arg^{258} and Arg^{283}, respectively (see Table 1).

In pol β, the movement of Arg^{258} has been proposed to be a slow, rate-limiting step in the conformational cycle (not the overall insertion pathway) based on computational studies (24,26,28). To determine whether Ile^{492} behaves analogously to Arg^{258} in pol β, two simulations from the binary state with Ile^{492} mutated to alanine in the presence of the incoming nucleotide were performed. To distinguish the contributions of the metal ions in the active site, one mutant simulation contains only the nucleotide-binding Mg^{2+} while the other contains both the nucleotide-binding and catalytic Mg^{2+} ions in the active site. The single-residue mutation of Ile^{492} may alter the enzyme's conformational closing and/or affect the chemistry step (if rate-limiting), thus changing the rate of nucleotide insertion.

We also explored behavior in a pol-λ complex with Arg^{517} mutated to alanine with both magnesium ions from the ternary state. Arg^{517} assumes a position similar to the base-checking Arg^{283} residue in the closed state of pol β. Because the x-ray crystal structure data indicate that the side chain of Arg^{517} interacts with both the templating base at the gap and the adjacent template base that pairs with the primer terminus in the ternary state before chemistry (1,32), an alanine substitution for Arg^{517} should disrupt these interactions.

Our combined simulations establish the importance of concerted DNA motions and rearrangements in transitioning active-site residue side chains from the binary to the ternary state of pol λ. Thus, our simulation work supports the existence of an inactive conformation of pol λ which transitions to an active conformation upon binding the correct incoming nucleotide; in this way, pol λ's conformational transitions support an induced-fit mechanism. We consider the inactive binary conformation ''open'' and the active ternary conformation ''closed'' since active-site residues, DNA, and the loop containing β-strand 8 in the thumb are only positioned for catalysis in the ternary conformation. Thus, open-to-closed terminology for pol λ does not coincide with large-scale subdomain motions alone. We also observe that placing the catalytic ion in the active site stimulates the transition from the binary to ternary state and produces a close interaction among the catalytic aspartates (Asp^{427}, Asp^{429}, Asp^{490}). The mutant trajectories illustrate the importance of Ile^{492} and Arg^{517} in the organization of the active site. The combined results suggest specific functions for several active-site residues (Ile^{492}, Phe^{506}, Tyr^{505}, Arg^{517}, Arg^{514}) and a sequence of events in the conformational transitions pathway of pol λ. As in pol β, these five residues may act as ''gate-keepers'' that regulate the transition of the enzyme-substrate complex to a chemically competent state.

COMPUTATIONAL DETAILS

Initial models

Eight initial models were prepared based on the crystal pol λ binary (PDB entry 1XSL) and ternary (PDB entry 1XSN) complexes. Five models represent wild-type pol λ forms while three are of mutated forms of pol λ. Four models were built from the binary crystal complex by placing the incoming nucleotide (dTTP) in the active site; in two of these models both the catalytic and nucleotide-binding Mg^{2+} ions were also placed in the active site. In the other two models, only the nucleotide-binding ion was also placed in the active site. The incoming nucleotide and nucleotide-binding ion were positioned by superimposing the protein C_α atoms with those in

TABLE 1 Key residues in pol λ and corresponding residues in pol β

Residue in pol λ	Corresponding residue in pol β	Function of pol-β residue	Function of pol-β residue (deduced from this study)
Tyr^{505}	Tyr^{271}	Interacts with templating base in open state.	Interacts with templating base in open state.
Phe^{506}	Phe^{272}	Blocks interaction between Arg^{258} and Asp^{192} in closed state.	Flip to closed state allows DNA motion toward closed-state position.
Ile^{492}	Arg^{258}	In open state, interacts with Asp^{192}; in closed state, hydrogen bonds with Tyr^{296} and Glu^{295}.	In open state, sterically inhibits flip of Phe^{506} to closed-state position.
Asp^{427}	Asp^{190}	Coordinates with both Mg^{2+} ions in closed state.	Coordinates with both Mg^{2+} ions in closed state.
Asp^{429}	Asp^{192}	In open state, interacts with Arg^{258}; in closed state, coordinates with both Mg^{2+} ions.	Coordinates with both Mg^{2+} ions in closed state.
Asp^{490}	Asp^{256}	Coordinates with the catalytic Mg^{2+} ion in the closed state.	Coordinates with the catalytic Mg^{2+} ion in the closed state.
Arg^{517}	Arg^{283}	In closed state, is adjacent to the templating base and may be responsible for checking for correct basepairing.	In closed state, maintains position of nascent basepair and stabilizes closed state.
Arg^{514}	Lys^{280}	In closed state, positions itself to stack with the templating base.	First residue to respond to thumb motion; in closed state, stacks with templating base.

the pol-λ ternary complex. The catalytic ion was positioned by superimposing the pol-λ protein C_α atoms onto those of the pol-β ternary complex (PDB entry 1BPY). The DNA sequences of both the template and primer strands were modified to match those of the pol-λ ternary complex. From the four models constructed from the binary crystal complex, one model containing only the nucleotide-binding ion and one model containing both the nucleotide-binding and catalytic Mg^{2+} ions in the active site were selected. In these two chosen models, residue Ile^{492} was mutated to alanine.

To test for the presence of an induced-fit mechanism and the role of the catalytic Mg^{2+} ion, three models from the ternary complex were prepared with the following configurations: both ions present, only the nucleotide-binding Mg^{2+} ion present, and without the presence of ions or dTTP in the active site pocket. The catalytic ion missing in the ternary crystal complex was similarly positioned by superimposing the C_α atoms of pol λ onto those of pol β's ternary structure. A fourth model of the ternary complex was also prepared with residue Arg^{517} mutated to alanine. This complex contained only the nucleotide-binding ion in the active site.

In the initial structures, missing protein residues 1–8 were added to the binary complex and residues 1–11 were added to the ternary complex. An oxygen atom was added to the 3′ carbon of the ddTTP sugar moiety in the ternary complex to form 2′,3′-deoxythymidine triphosphate (dTTP). All other missing atoms from the x-ray crystal structures were also added to our binary and ternary models. Mutant residue Ala^{543} of the ternary protein was also replaced with Cys^{543} to reflect the natural amino-acid sequence found in the binary complex protein.

Optimized periodic boundary conditions in a cubic cell were introduced to all complexes using the PBCAID program (41). The smallest image distance between the solute, the protein complex, and the faces of the periodic cubic cell was 10 Å. To obtain a neutral system at an ionic strength of 150 mM, the electrostatic potential of all bulk-water (TIP3 model) oxygen atoms was calculated using the Delphi package (42). Those water oxygen atoms with minimal electrostatic potential were replaced with Na^+ and those with maximal electrostatic potential were replaced with Cl^-. All Na^+ and Cl^- ions were placed at least 8 Å away from both protein and DNA atoms and from each other.

Both the initial binary and ternary models contain ~38,325 atoms, 278 crystallographically resolved water molecules from the binary complex, 10,481 bulk water molecules, Mg^{2+} ions, incoming nucleotide dTTP, and 41 Na^+ and 29 Cl^- counterions. The final dimensions of the box are: 72.61 Å × 75.97 Å × 70.91 Å.

Minimization, equilibration, and dynamics protocol

Eight simulations were performed as summarized in Table 2 and as proposed above. Initial energy minimizations and equilibration simulations were performed using the CHARMM program (37) with the all-atom C26a2 force field (43). First, each system was minimized with fixed positions for all heavy atoms except those from the added residues using SD for 5000 steps followed by ABNR for 10,000 steps. Two cycles of further minimization were carried out for 10,000 steps using SD followed by 20,000 steps of ABNR. During minimization, all atoms except those of Cl^-, Na^+, and water were kept fixed allowing the water molecules to relax around the protein/DNA complex. The equilibration process was started with a 30-ps simulation at 300 K using single-timestep Langevin dynamics and keeping the constraints used in the previous minimization step. The SHAKE algorithm was employed to constrain the bonds involving hydrogen atoms. This was followed by unconstrained minimization using 10,000 steps of SD followed by 20,000 steps of ABNR. A further 30 ps of equilibration at 300 K and minimization consisting of 2000 steps of SD followed by 4000 steps of ABNR were performed. The final equilibration step involved 130 ps dynamics at 300 K.

TABLE 2 Summary of simulations performed before chemistry

Simulation No.	System	Magnesium ions in active site	Incoming nucleotide in/near active site
1	Binary wt	Nuc	Present
2	Binary wt	Nuc + cat	Present
3	Ternary wt	Nuc	Bound
4	Ternary wt	Nuc + cat	Bound
5	Ternary wt	None	None
6	Binary I492A	Nuc	Present
7	Binary I492A	Nuc + cat	Present
8	Ternary R517A	Nuc	Bound

Key: *nuc*, nucleotide-binding ion; *cat*, catalytic ion; *wt*, wild-type.

Production dynamics were performed using the program NAMD (44) with the CHARMM force field (43). First, the energy in each system was minimized with fixed positions for all protein and DNA heavy atoms using the Powell algorithm. Systems were then equilibrated for 100 ps at constant pressure and temperature. Pressure was maintained at 1 atm using the Langevin piston method (45), with a piston period of 100 fs, a damping time constant of 50 fs, and piston temperature of 300 K. Temperature coupling was enforced by velocity reassignment every 2 ps. Then, production dynamics were performed at constant temperature and volume. The temperature was maintained at 300 K using weakly coupled Langevin dynamics of non-hydrogen atoms with damping coefficient $\gamma = 10\ ps^{-1}$ used for all simulations performed; bonds to all hydrogen atoms were kept rigid using SHAKE (46), permitting a time step of 2 fs. The system was simulated in periodic boundary conditions, with full electrostatics computed using the PME method (47) with grid spacing on the order of 1 Å or less. Short-range nonbonded terms were evaluated every step using a 12 Å cutoff for van der Waals interactions and a

smooth switching function. The total simulation length for all systems was 20 ns.

Simulations using the NAMD package were run on NCSA's Tungsten Xeon Linux Cluster at University of Illinois at Urbana-Champaign and local SGI Altix 3700 Intel Itanium-2 processor shared-memory systems running the Linux operating system.

RESULTS

Wild-type pol-λ systems

No substantial thumb subdomain motions

Overall, none of our wild-type simulations of pol λ reveal substantial subdomain motion to/from the binary or ternary conformations, although rotation of the loop containing β-strand 8 in the thumb subdomain occurs in the simulations started from the binary state. Specifically, no significant changes in the palm (β-strands 3 and 4 and connecting loop) are detected over 20 ns of simulation time in all wild-type pol-λ trajectories performed. Fig. 2 *a* shows the positions of the simulated palm subdomains compared to the crystal states.

From the binary state (Simulation 1, Table 2) with dTTP and only the nucleotide-binding ion added, the thumb (loop containing β-strand 8) remains open throughout the simulation, although some fluctuations occur. Note that Fig. 2 *a* shows the final conformations of simulated pol λ superimposed along the C_α trace with the crystal binary and ternary pol-λ structures; and Fig. S1 *a* (Supplementary Material) shows the RMSD of C_α atoms located in the loop containing β-strand 8 in the thumb relative to those same atoms of the crystal binary and ternary structures.

A downward movement of the thumb subdomain, particularly in the loop containing β-strand 8, occurs in the trajectory of the binary state with dTTP and both the catalytic and nucleotide-binding Mg^{2+} ions added to the active site of the enzyme (Simulation 2) (Fig. 2, *a* and *b*). This movement, however, is not toward the ternary position but in the opposite direction, keeping the enzyme in a more open conformation, as is evident in Fig. S1 *b* showing the RMSD of C_α atoms located in this loop in the thumb relative to those same atoms of the crystal binary and ternary structures.

From the ternary state (Simulations 3–5), no substantial movement of the loop containing β-strand 8 in the thumb subdomain was observed. (Fig. 2, *a* and *b*, show the simulated structures after 20 ns, and Fig. S2, *a–c*, show plots of the RMSD of C_α atoms from the β-strand 8 containing loop in the thumb in all the ternary simulations relative to those same atoms of the crystal binary and ternary structures.)

A closing motion of the loop containing β-strand 8 in the thumb subdomain was observed in one of our mutation simulations (Simulation 7), which is described in detail below under Mutant Systems.

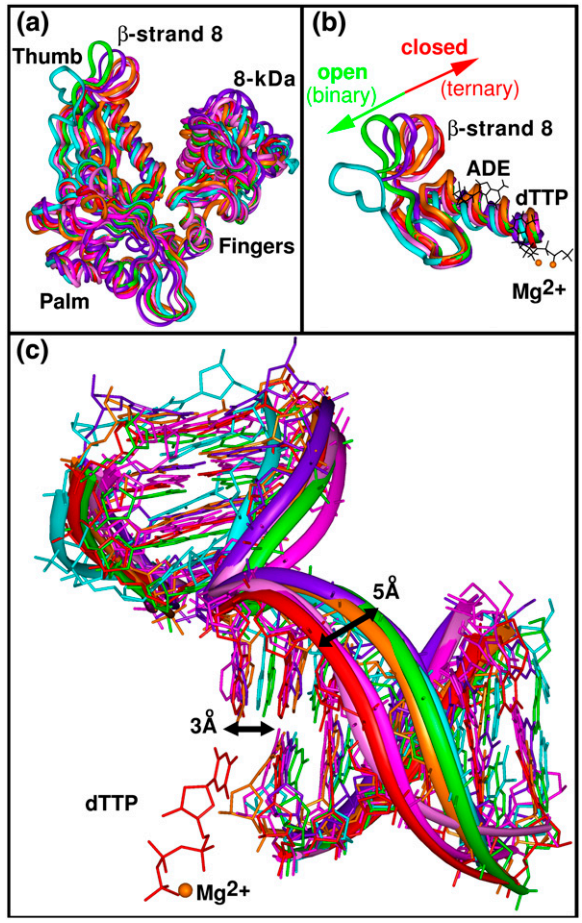

FIGURE 2 Subdomain and DNA motion in wild-type DNA pol λ simulations. Simulations 1 (*purple*), 2 (*cyan*), 3 (*magenta*), 4 (*pink*), and 5 (*orange*); see Table 2. (*a*) All final states from the 20-ns simulated wild-type proteins superimposed along the C_α trace with crystal binary (PDB entry 1XSL, *green*) and ternary (PDB entry 1XSN, *red*) structures. Only residues 323–575 are shown for clarity. (*b*) Enlarged view of motion in the loop containing β-strand 8 in the thumb subdomain. Protein residues 509–545 are shown. Watson-Crick basepairing between the templating base and dTTP with both catalytic and nucleotide-binding Mg^{2+} ions present are included from Simulation 4; hydrogens have been removed for clarity. (*c*) DNA position in the crystal binary (PDB entry 1XSL, *green*) and ternary (PDB entry 1XSN, *red*) states as well as the DNA positions in all simulations of wild-type pol λ after 20 ns. Key distances between crystal binary and ternary states are also provided. Only the crystal ternary dTTP and Mg^{2+} are shown. Hydrogens are omitted for clarity.

DNA shift motions in binary systems and ternary complex without ions

In contrast to the absence of significant subdomain motion, we observe DNA motions in all wild-type simulations except Simulations 3 and 4 and mutant Simulations 7 and 8.

In the trajectory started from the ternary state without the dTTP and the Mg^{2+} ions (Simulation 5), we observe a shift in the DNA template strand toward the binary position (Fig. 2 *c*). The templating base at the gap, however, has not shifted to the binary position. In Fig. S3 *c*, the plot of the RMSD of

DNA backbone atoms from those same atoms of the crystal binary and ternary complexes indicates that movement has occurred away from the crystal ternary position and toward the crystal binary position.

A movement of the templating base at the gap toward the ternary position occurs in both simulations started from the binary state with substrate added (Simulations 1 and 2). The backbone of the template strand, however, does not move from the binary position in either simulation (Fig. 2 *c*). Thus, the plots of the RMSD of DNA backbone atoms relative to those atoms of the crystal binary and ternary complexes shown in Fig. S4, *a* and *b*, do not indicate convergence of the DNA toward the ternary position. Simulations 3 and 4 (ternary, with one or both ions) do not reveal substantial DNA shifts (Figs. 2 *c* and S3), likely because the DNA is already in the appropriate position for the nucleotidyl transfer reaction to occur.

We conclude that DNA motion is one of the primary responses of the pol λ/DNA complex to the presence or absence of substrate in the active site. Interestingly, simulations performed on another low-fidelity DNA polymerase, Dpo4, from the Y-family, exhibit DNA sliding by one basepair but suggest that the motion occurs after the chemistry step to prepare the system for the next reaction cycle (48). In pol λ, the full movement of the DNA molecule does not occur in one step. In fact, our simulations suggest that the DNA template backbone motion and the change of the template base positions can occur independently. Moreover, pol λ's movement of the DNA template strand from the ternary to binary positions does not depend on motion of the loop containing β-strand 8 in the thumb subdomain: in Simulation 5, the template strand moves back to the binary position, but no thumb-loop motion occurs. The fluctuations in the thumb loop observed in our binary simulations with substrate added may allow for minor motion of the DNA toward the ternary position. Further evidence of the influence of motion of the loop containing β-strand 8 in the thumb on the transition of the DNA from the binary to ternary positions is found in our mutant simulation results.

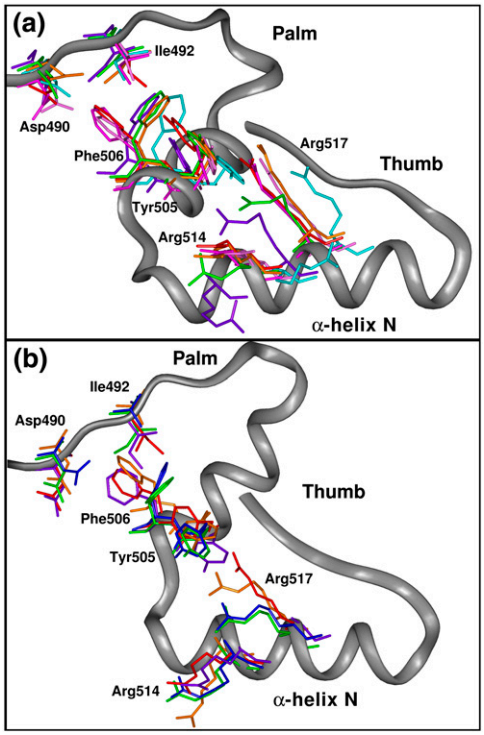

FIGURE 3 Residue side-chain orientations in the crystal binary (PDB entry 1XSL, *green*) and ternary (PDB entry 1XSN, *red*) pol-λ complexes as well as in all simulations performed. (*a*) Positions of key residues in crystal binary and ternary states and in all simulations of wild-type pol λ after 20 ns. Simulations 1 (*purple*), 2 (*cyan*), 3 (*magenta*), 4 (*pink*), and 5 (*orange*); see Table 2. (*b*) Positions of key residues in crystal binary and ternary states and in all simulations of mutated forms of pol λ after 20 ns. Simulations 6 (*blue*), 7 (*orange*), and 8 (*purple*); see Table 2.

Local rearrangements of active site residues

Associated with subdomain motions are changes in the orientations of specific residues in the active site as shown in Fig. 3 *a*. The key residues Tyr^{505}, Phe^{506}, Ile^{492}, Arg^{517}, Arg^{514}, Asp^{427}, Asp^{429}, and Asp^{490} correspond to residues Tyr^{271}, Phe^{272}, Arg^{258}, Arg^{283}, Lys^{280}, Asp^{190}, Asp^{192}, and Asp^{256}, respectively, in pol β (see Table 1). From a detailed analysis of the available crystal structures, we can determine that Tyr^{505}'s side chain blocks an incoming dNTP from basepairing with the templating base in the gap in the binary complex but moves away from the gap in the ternary complex; this change in position likely causes a rotation in the side chain of neighboring Phe^{506}. Arg^{517} moves from stacking with the templating base in the binary complex to a location similar to that of Arg^{283} in the closed form of pol β. (Arg^{283} in pol β is responsible for maintaining correct basepairing (9,49–51)). As pol λ's Arg^{517} moves away from the DNA, Arg^{514} assumes a position similar to that taken by Arg^{517} and stacks with the templating base, a movement seen in pol β's active site by Lys^{280}.

Fig. 3 *a* shows the orientations of these residues in the last frame of all wild-type pol-λ trajectories compared to the positions of the crystal binary and ternary residues. The positions of Ile^{492} and Tyr^{505} are much closer to the binary position than the ternary position, even in Simulations 3 and 4 started from the ternary state with substrate bound. The flip of Ile^{492} occurs early (~1.5 ns) in Simulation 3, which contains the nucleotide-binding ion, but only ~18 ns in simulation 4 started from the ternary state with the catalytic ion added.

Fig. 3 *a* shows that the initial position of Phe^{506} remains the same throughout all simulations of wild-type pol λ with the exception of Simulation 5 where dTTP and Mg^{2+} have been removed from the ternary state. There, Phe^{506} along with Ile^{492} and Tyr^{505} flip from the ternary to the binary state orientations. Interestingly, this is the same simulation that

shows DNA template strand movement, suggesting that the flip of these residues is correlated with DNA motion.

In our simulations of wild-type pol λ from the binary state, movement occurs in the side chains of Arg^{514} and Arg^{517}. In Simulation 1, with dTTP and the nucleotide-binding Mg^{2+}, Arg^{514} moves from its initial position of the binary state, but not directly toward the ternary state position (Fig. 3 *a*). In Simulation 2, Arg^{517} rotates significantly from its initial position toward the ternary state while Arg^{514} appears to move to an intermediate position during the simulation. The movements of Arg^{514} and Arg^{517} are correlated with the motion of the loop containing β-strand 8 in the thumb subdomain. In comparison, all simulations of wild-type pol λ starting from the ternary state show no thumb subdomain motion, and both Arg^{517} and Arg^{514} maintain their positions over the 20 ns of simulation time.

Thus, our simulations reveal that when dTTP is removed from the ternary state, several residue flips occur toward positions corresponding to the binary state (i.e., Ile^{492}, Tyr^{505}, and Phe^{506}). These movements also permit some partial DNA movement toward the binary state. We infer that movements in residues 514 and 517 depend on thumb subdomain motion, since residue movement only occurs after such motion.

Small ion-dependent magnesium ion coordination adjustments

Previous studies have shown that both the catalytic and nucleotide-binding ions stabilize the closed active site conformation and prepare it for the nucleotidyl transfer reaction after the correct nucleotide binds (27,28,35,40,52). Since only the nucleotide-binding Mg^{2+} ion is observed in the ternary x-ray crystal structure of pol λ (PDB entry 1XSN), we placed the catalytic Mg^{2+} ion in the active site in our simulations starting from both the binary and ternary states to observe its effect on the assembly of the active site for the nucleotidyl transfer reaction.

Fig. 4 shows the Mg^{2+} ion coordination with nearby active site residues after 20 ns from Simulations 1–4 of pol λ in the presence of the correct substrate. Table 3 provides distance data related to the Mg^{2+} ion coordination.

Fig. 4, *c* and *d*, show that the addition of the catalytic Mg^{2+} ion to the ternary system produces adjustments in the active site to accommodate the additional catalytic Mg^{2+} ion. The side chains of residues Asp^{427}, Asp^{429}, and Asp^{490} flip to coordinate with the catalytic ion; two water molecules also enter the active site to coordinate with the catalytic ion while one water molecule coordinates with the nucleotide-binding ion. These coordinating waters are also present in our simulations started from the binary state. In addition, a third water molecule coordinates with the catalytic Mg^{2+} ion, and slight adjustments of Asp^{427} and Asp^{429} occur to allow better coordination with the catalytic ion (Fig. 4, *a* and *b*). However, the flip of Asp^{490} is not captured during 20 ns.

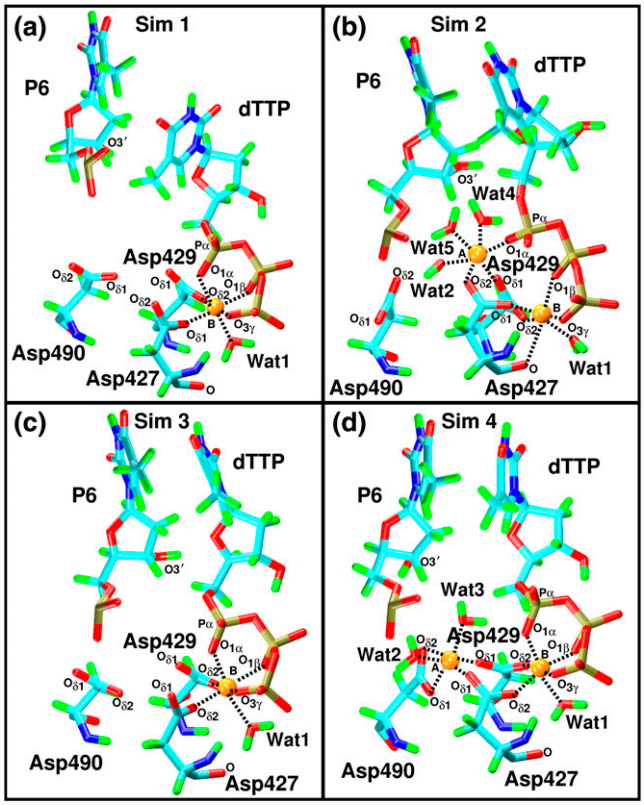

FIGURE 4 Active site arrangements from all simulations of wild-type pol λ with substrate (dTTP) present (Simulations 1–4, Table 2). The coordinations of the catalytic Mg^{2+} ion (*A*) and nucleotide-binding Mg^{2+} ion (*B*) with surrounding atoms are depicted by the dashed lines. Water molecules are included.

This is consistent with the sequence of events observed in simulations of pol β where one catalytic aspartate, Asp^{192}, is slow to move into the active site to coordinate with the catalytic ion (28). Thus, the active sites of simulations started from the binary state are not assembled for the nucleotidyl transfer reaction after 20 ns.

As anticipated, in all simulations performed, the presence of the catalytic ion produces a close arrangement of the catalytic aspartates (Asp^{427}, Asp^{429}, and Asp^{490}) in the active site where the metal ions are hexacoordinated. Simulation 4, however, started from the ternary state, shown in Fig. 4 *d*, appears to be the closest to a reaction-competent state since its active site exhibits the tightest arrangement of the catalytic aspartates and Asp^{490} coordinates with the catalytic ion.

Mutant systems

Recall (see Introduction) that two simulations of pol λ from the binary state for $Ile^{492}Ala$ (Simulations 6 and 7, with the nucleotide-binding ion or both ions) were performed to assess the role of Ile^{492} in the transition from the binary to the ternary states and determine how system behavior depends on the presence of the catalytic ion, and that one simulation

TABLE 3 Average active site interatomic distances for pol λ as observed during the last 1-ns of simulations and from x-ray crystal structure (PDB entry 1XSN)

Distance (Å)	Sim. 1	Sim. 2	Sim. 3	Sim. 4	Ternary (1XSN)
Nucleotidyl transfer distance					
dTTP (Pα) : P6 (O3′)	7.86	4.76	4.68	6.14	n/a
Distance between magnesium ions					
Mg^{2+}(A) : Mg^{2+}(B)	n/a	4.16	n/a	4.35	n/a
Catalytic magnesium ion coordination					
Mg^{2+}(A) : Asp^{427} ($O_{\delta1}$)	n/a	3.17	n/a	1.82	n/a
Mg^{2+}(A) : Asp^{427} ($O_{\delta2}$)	n/a	1.86	n/a	3.50	n/a
Mg^{2+}(A) : Asp^{429} ($O_{\delta1}$)	n/a	1.83	n/a	1.85	n/a
Mg^{2+}(A) : Asp^{490} ($O_{\delta1}$)	n/a	6.05	n/a	1.92	n/a
Mg^{2+}(A) : Asp^{490} ($O_{\delta2}$)	n/a	4.15	n/a	1.91	n/a
Mg^{2+}(A) : Wat2 (OH2)	n/a	2.03	n/a	2.10	n/a
Mg^{2+}(A) : Wat3 (OH2)	n/a	n/a	n/a	1.98	n/a
Mg^{2+}(A) : Wat4 (OH2)	n/a	2.05	n/a	n/a	n/a
Mg^{2+}(A) : Wat5 (OH2)	n/a	2.08	n/a	22.7	n/a
Mg^{2+}(A) : dTTP ($O1_{\alpha}$)	n/a	1.84	n/a	3.85	n/a
Mg^{2+}(A) : P6 (O3′)	n/a	4.92	n/a	4.73	n/a
Nucleotide magnesium ion coordination					
Mg^{2+}(B) : Asp^{427} ($O_{\delta1}$)	1.85	1.83	3.36	3.55	3.62
Mg^{2+}(B) : Asp^{427} ($O_{\delta2}$)	3.50	3.79	1.86	1.84	2.00
Mg^{2+}(B) : Asp^{427} (O)	4.02	2.20	4.07	4.03	3.94
Mg^{2+}(B) : Asp^{429} ($O_{\delta2}$)	1.89	1.86	1.86	1.88	2.13
Mg^{2+}(B) : Wat1 (OH2)	2.05	2.05	2.04	2.07	n/a
Mg^{2+}(B) : Wat6 (OH2)	n/a	n/a	n/a	n/a	2.15
Mg^{2+}(B) : dTTP ($O1_{\beta}$)	1.91	1.83	1.91	1.92	1.88
Mg^{2+}(B) : dTTP ($O1_{\alpha}$)	1.90	3.74	1.92	1.90	1.98
Mg^{2+}(B) : dTTP ($O3_{\gamma}$)	1.84	1.82	1.86	1.85	2.20

Key: Mg^{2+}(A), catalytic ion; Mg^{2+}(B), nucleotide-binding ion; dTTP, 2′-deoxythymidine 5′-triphosphate; P6, primer terminus; Wat1, Wat2, Wat3, Wat4, Wat5, Wat6, water molecules; n/a, not available.

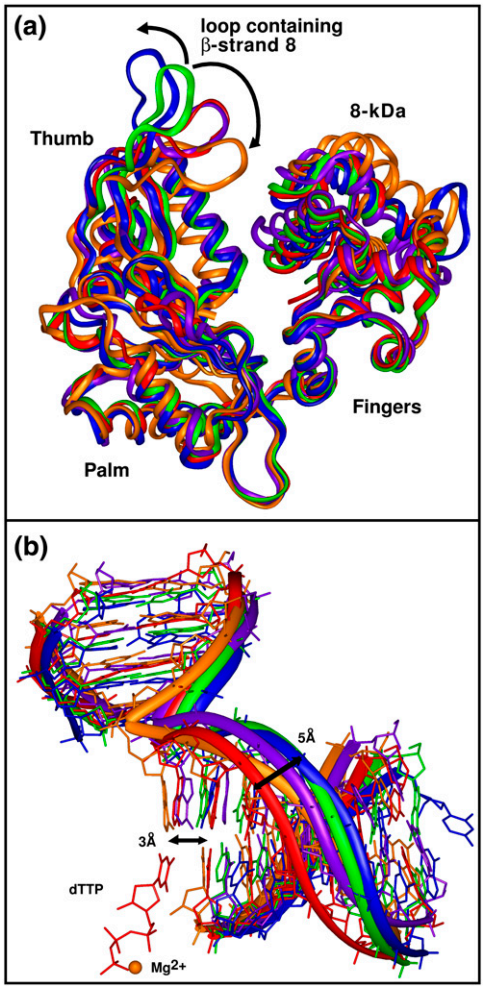

FIGURE 5 Subdomain and DNA motion in mutant DNA pol λ simulations. Simulations 6 (*blue*), 7 (*orange*), and 8 (*purple*), Table 2. (*a*) Subdomain motion in mutant simulations of DNA pol λ. All simulated mutated forms of pol λ are shown after 20 ns, superimposed along the C_{α} trace with crystal binary (PDB entry 1XSL, *green*) and ternary (PDB entry 1XSN, *red*) structures. Only residues 323–575 are shown for clarity. Arrows represent thumb loop motion from the initial binary conformation in Simulations 6 and 7. (*b*) DNA position in the crystal binary (PDB entry 1XSL, *green*) and ternary (PDB entry 1XSN, *red*) states as well as the DNA positions in all simulations of mutated forms of pol λ after 20 ns. Key distances between crystal binary and ternary states are also provided. Only the crystal ternary dTTP and Mg^{2+} are shown. Hydrogens have been removed from all simulated structures for clarity.

from the ternary state for Arg^{517}Ala with only the nucleotide-binding ion was performed (Simulation 8) to clarify Arg^{517}'s effect on the formation of a correct basepair and stabilization of the active site for the nucleotidyl transfer reaction.

Fig. 5 *a* shows the conformations of the proteins at the end of the 20 ns simulations superimposed with the crystal binary and ternary protein structures. For the Ile^{492} system 7, with dTTP and both ions, thumb loop closing motion occurs. The altered position of α-helix N can be attributed to thermal fluctuations. No thumb subdomain motion is observed in Simulation 6 started from the binary state of the Ile^{492}Ala mutant and Simulation 8 started from the ternary state for the Arg^{517}Ala mutant, both with dTTP and only the nucleotide-binding ion. The thumb loop motion occurring in Simulation 7 and the lack of motion observed in Simulations 6 and 8 can be seen in Fig. S1, *d* and *c*, and Fig. S2 *d*, respectively. These figures show the RMSD of C_{α} atoms located in the loop containing β-strand 8 in the thumb relative to those same atoms of the crystal binary and ternary states. Paralleling our observations in the wild-type simulations, no significant changes in positions of β-strands 3 and 4 in the palm subdomain occur in any mutant simulations (Fig. 5 *a*).

In mutant Simulations 7 and 8, DNA motion is observed (Fig. 5 *b*). In Simulation 7, this consists in a shift in the base at the gap from the binary position to the ternary position. The template DNA strand also partially moves from the starting binary position to the ternary position. This motion can also be seen in Fig. S4 *d*, which shows the RMSD of the simulated DNA backbone atoms relative to those atoms of the crystal binary and ternary states. For Simulation 8, both the DNA template strand and the base at the gap move from the ternary position to the binary position. However, by

the end of the simulation, the templating base at the gap returns to its starting ternary position. This wavering motion is evident from Fig. S4 *d*, which shows the RMSD of the simulated DNA backbone atoms relative to those atoms in the crystal binary and ternary states.

Our combined thumb/DNA motion results indicate that like for wild-type pol λ, DNA template strand motion from the ternary to binary states does not require motion of the loop containing β-strand 8 in the thumb subdomain. Our results from Simulation 7 reveal that thumb loop closing motion may assist in the repositioning of the DNA when moving from the binary to the ternary state since the loop containing β-strand 8 in the thumb increases in proximity to the DNA template strand backbone. This is similar to simulations of Dpo4 where the little finger subdomain guides the translocation of the DNA (48).

Active-site residue motions also occur in the mutant simulations. Fig. 3 *b* shows the final positions of Asp^{490}, Ile^{492}, Tyr^{505}, Phe^{506}, Arg^{514}, and Arg^{517} in all three mutant simulations (6–8) compared to the residues of the crystal binary and ternary structures. In Simulation 7 (I492A system with both ions), Phe^{506} flips to the ternary state, but Tyr^{505} and Arg^{517} are in intermediate orientations between the binary and ternary states by the end of the simulation. Residue Arg^{514} adopts a position away from its binary and ternary positions similar to that observed in Simulation 1 started from the binary conformation. Interestingly, Asp^{490} in Simulation 7, which does not coordinate with the catalytic ion, is closer to the active site than it is in Simulation 6 (I492A system without the catalytic ion), where it flips away from the other catalytic aspartates. This supports the hypothesis that the presence of the catalytic ion assists in the tighter arrangement of the residues in the active site. In Simulation 8 (R517A system), both Ile^{492} and Tyr^{505} flip to the binary orientations while residues Phe^{506} and Arg^{514} remain in their initial ternary conformations.

While we expect that replacement of Ile^{492} with alanine might influence conformational transitions, we did not anticipate that the mutation would have such far-reaching effects on neighboring residues, DNA, and thumb subdomain. Clearly, Ile^{492} plays a critical role in directing conformational changes in the transition from the binary to ternary states. The effect of the mutation, however, is modulated by the presence or absence of the catalytic ion, since these conformational changes do not occur in Simulation 6 where the catalytic ion is absent.

Simulation 8 supports our hypothesis that Arg^{517} is essential for maintenance of the correct basepair alignment. We did not expect, however, that the position of the DNA would vary in the absence of the arginine side chain. The enzyme-substrate complex, otherwise, seems very stable as anticipated from mutation studies of pol β where Arg^{283}, the corresponding residue to pol λ's Arg^{517}, mutated to alanine or lysine, was found to have no affect on the global conformation of the enzyme (53).

DISCUSSION

Our simulations of pol λ indicate that its catalytic cycle follows an induced-fit mechanism since the pol λ/DNA complex transitions from an open (inactive) conformation to a closed (active) conformation upon binding the correct substrate. A summary of the conformational changes we observed is collected in Table 4. In contrast to pol β, pol λ exhibits only minor thumb subdomain motions during this transition. The thumb motion, localized to a loop, also depends on the presence of the catalytic Mg^{2+} in the active site, consistent with a ''two-metal-ion'' mechanism, since no closing motion was detected when the incoming nucleotide and only the nucleotide-binding Mg^{2+} ion were present in the active site. Because significant transitions toward the active ternary state occur in our simulations, large-scale subdomain motions do not appear to be a part of the catalytic cycle of pol λ. Based on comparison with other dynamics studies of DNA polymerases, such as Dpo4 (48) and pol β (25), the length of our pol-λ simulations is not likely a major factor that can explain the different observations. Of course, we cannot exclude the possibility that on longer timescales other transitions will occur.

Previous studies on pol β have established that the transition between the open and closed conformations involves a directed, sequential reorientation of certain active site residues (31). These repositioned residues assist in preparing the enzyme-substrate complex for the nucleotidyl transfer reaction by maintaining a proper hydrogen-bonding network with the water molecules, ions, and the incoming dNTP. As seen through our simulations, pol-λ active site residues are also very important in the transition to the active ternary state.

To reach a reaction-competent state, DNA movements as well as residue side-chain adjustments near the active site are necessary. A DNA shift to the ternary position and thumb loop closing occur in the simulation of Ile^{492}Ala from the binary state when substrate is added (Simulation 7). In

TABLE 4 Summary of DNA and protein motions in all simulations

	DNA motions*		Protein motions*	
Simulation No.	Template strand	Template base (Ade)	Residues that flip	Loop containing β-strand 8
1	Binary	Ternary	Arg^{514}	Binary
2	Binary	Toward ternary	Arg^{514}, Arg^{517}	Binary
3	Ternary	Ternary	Ile^{492}, Tyr^{505}	Ternary
4	Ternary	Ternary	Asp^{490}, Ile^{492}, Tyr^{505}	Ternary
5	Binary	Ternary	Ile^{492}, Tyr^{505}, Phe^{506}	Ternary
6	Binary	Binary	Asp^{490}	Binary
7	Ternary	Ternary	Tyr^{505}, Phe^{506}, Arg^{514}, Arg^{517}	Ternary
8	Binary	Ternary	Ile^{492}, Tyr^{505}	Ternary

*The terms *Binary* and *Ternary* indicate the position that is approached in each simulation in reference to the binary (1XSL) or ternary (1XSN) crystal structures.

Simulation 5, started from the ternary state of pol λ with the substrate removed, the DNA moves toward the binary position without perturbing the global conformation of the enzyme. Active site residues (Asp^{427}, Asp^{429}, Asp^{490}, Ile^{492}, Tyr^{505}, Phe^{506}, Arg^{514}, and Arg^{517}) also flip in many simulations in response to (the presence or absence of) substrate and Mg^{2+} ions in the active site. These rearrangements may help regulate the catalytic pathway of pol λ since large scale subdomain motions are absent. Our mutation studies indicate that Ile^{492} and Arg^{517} have a major effect on the assembly of the active site. Since pol λ has fewer interactions with the DNA than pol β (33), the importance of these residues is elevated.

Interestingly, analyses reveal similarities between pol λ and both pol β and pol X in that further adjustments are still needed to reach a reaction-competent state in the active site of the ternary complex in the presence of both ions (27,54–56). These changes lie within the ''pre-chemistry avenue'' (27) previously proposed for pol β. The conformational changes required include a movement in the position of the catalytic Mg^{2+} ion to bring the primer terminus P6 : O3′ and dTTP : P_α atoms closer together, since the nucleotidyl transfer distance is, on an average, ~6.1 Å during the last nanosecond of the simulation (see Table 3). In general, the observed magnesium ion coordination distances with respect to the surrounding active site residue atoms are larger than those observed in computational studies of pol β (25). This further organization of the active site is necessary to fully evolve the enzyme-substrate complex to a reaction-competent state.

A careful analysis of all data suggests specific roles of several residues (Ile^{492}, Tyr^{505}, Phe^{506}, Arg^{514}, and Arg^{517}) in the active site, as detailed below and summarized in Table 1. The orientations of these residues are strongly correlated to the position of the DNA, and these residues may be primarily responsible for correctly positioning the nascent basepair and the primer terminus basepair for the nucleotidyl transfer reaction.

Ile^{492}

Pol λ's Ile^{492}, an analog of pol β's Arg^{258}, appears to play a role in the transition from the binary to ternary states by determining the position of neighboring residue Phe^{506} (Phe^{272} in pol β). Specifically, Ile^{492} in the binary form sterically inhibits the flipping motion of Phe^{506} to the ternary position. Evidence for this hypothesis comes from a cumulative analysis of our simulations of wild-type pol λ as well as from our mutation simulation of the pol λ Ile^{492}Ala mutant. In our wild-type simulations of pol λ started from the binary state (Simulations 1 and 2), no movement of Ile^{492} or Phe^{506} was observed. In our wild-type simulations of pol λ started from the ternary state with substrate present (Simulations 3 and 4), Ile^{492} flips from the ternary to the binary state, while Phe^{506} remains unaffected. In Simulation 5 from the ternary state without substrate, Ile^{492} flips from the ternary to the binary position after the flip of Phe^{506} to the binary position. In the mutant simulation with both metal ions (Simulation 7), Phe^{506} easily flips to the ternary position and thumb loop closing motion occurs. That this flip of Phe^{506} does not occur in the other Ile^{492}Ala mutant trajectory (Simulation 6) further supports our hypothesis that the flip of Phe^{506} and thumb loop motion are strongly correlated to the presence of both ions in the active site. Interestingly, unlike Ile^{492}'s corresponding pol β residue Arg^{258} whose position determines whether or not neighboring catalytic Asp^{192} can coordinate with the catalytic ion (57), Ile^{492}'s position does not seem to affect the position of neighboring catalytic Asp^{490} (Asp^{256} in pol β), since it is unable to form a salt bridge with the aspartate. The position of Asp^{490} seems largely to be governed by the presence or absence of the catalytic ion. When the catalytic ion is absent, Asp^{490} can flip farther away from the active site as in Simulations 5 and 6. When the catalytic ion is present, Asp^{490} remains close to the active site (as seen in Simulations 2 and 7) or flips to coordinate with the catalytic ion (Simulation 4).

Phe^{506}

Residue Phe^{506} (Phe^{272} in pol β) governs the position of the DNA: DNA motion can only occur after Phe^{506} flips. This coupled Phe^{506} flipping with DNA movement was observed in Simulation 5 (ternary state without substrate) and in Simulation 7 (Ile^{492}Ala mutant with incoming nucleotide and both ions) during the transition from ternary to binary and from binary to ternary, respectively. Since thumb loop closing was only observed in Simulation 7, Phe^{506} may also be coupled to thumb subdomain motion as is the case for Phe^{272} (57). The importance of Phe^{506} gains support from experiments of mutated forms of pol λ (Phe^{506}Arg and Phe^{506}Gly) that exhibit very low polymerization activity as well as depressed processivity of DNA synthesis (58). Mutation studies of Phe^{272} indicate that the analog in pol β is important during ground-state binding in the selection of the correct nucleotide (59). Further evidence of the importance of this residue is that it is also conserved in pol X, where it is referred to as Phe^{116} (54).

Tyr^{505}

In addition, Phe^{506} indirectly affects the conformation of the DNA through its interactions with neighboring residue Tyr^{505} (Tyr^{271} in pol β), which directly contacts the bases of the DNA. Like Tyr^{271} in pol β, Tyr^{505} responds to the presence of an incoming nucleotide in the active site by moving away from the templating base. As shown in Fig. 3, *a* and *b*, Tyr^{505} assumes a position closer to that of the binary crystal state in all our simulations. This figure also shows that Tyr^{505}'s position is constrained by both adjacent Phe^{506} and nearby Arg^{517}. For example, in Simulation 2, Phe^{506} is positioned closer toward the binary and ternary crystal

positions of Tyr^{505} and so Tyr^{505} has moved away from Phe^{506} closer toward the ternary crystal position of Arg^{517}. This adjustment is allowed because the Arg^{517} residue has not yet fully moved to its ternary crystal position.

Mutation studies of Tyr^{505} replaced with alanine indicate that the polymerization activity is only mildly affected (58). Experimental data also indicate that Tyr^{505} may serve as a steric check on the size of the incoming nucleotide (60). In addition, mutation studies of Tyr^{271} suggest these steric considerations on the pol-β binding site since nucleotide binding affinities increase when Tyr^{271} is mutated to alanine and remain the same when it is mutated to similarly-sized phenylalanine (14). Thus, pol λ's Tyr^{505} is intricately connected to its neighboring residues and likely plays a role in the fidelity of the enzyme.

Arg^{517}

Residue Arg^{517} (Arg^{283} in pol β) also emerges as a key residue, as it helps stabilize the ternary state via interactions with the DNA bases. This was observed in our wild-type simulations of pol λ from the ternary state with substrate present (Simulations 3 and 4) where Arg^{517} stabilizes the DNA and thus little movement was shown. Without the substrate (Simulation 5), Arg^{517} remains in the ternary position throughout the simulation as did the template base at the gap, although the backbone of the template strand moves to the binary position. In our Arg^{517}Ala mutant trajectory (Simulation 8), the DNA backbone and template base moves temporarily from the ternary to the binary conformation since arginine's interactions with the DNA have been lost.

Pol β's Arg^{283} has a crucial role in the assembly of the active site as seen by an Arg^{283}Ala study reporting a 160-fold decrease in the fidelity of the mutant enzyme compared to the wild-type polymerase (50). A subsequent experimental study revealed how Arg^{283}'s interactions with the DNA minor groove account for the enzyme's specificity (49). Interestingly, mutations of Arg^{283} to other residues such as alanine or lysine have been found to greatly affect pol β's frameshift fidelity (61). Based on our simulation results, pol λ's Arg^{517} likely plays a key role in the enzyme's fidelity as does pol β's critical base-checking residue, Arg^{283}.

Arg^{514}

Arg^{514} (Lys^{280} in pol β) is the first to move away from the binary toward the ternary position when thumb loop motion occurs. In Simulation 7 of the binary state with substrate and both ions added, the thumb loop closes and Arg^{514} moves toward the ternary position. This makes room for Arg^{517} to begin its transition from the binary to ternary state. Movement of Arg^{514} in both Simulation 1 and 2 from the binary state is also accompanied by some movement of the templating base at the gap, suggesting that in addition to Phe^{506}, Tyr^{505}, and Ile^{492}, rearrangement of Arg^{514} facilitates the shift of the DNA from the binary to the ternary positions.

We can piece all these details together in a proposed conformational transition pathway for pol λ from the binary to ternary states (see Fig. 6): The binding of the correct dNTP stimulates the closing motion of the loop containing β-strand 8 in the thumb subdomain. This motion initiates the movement of Arg^{514}, which transitions to an intermediate conformation between the binary and ternary states. Arg^{517} then also flips close to its ternary state position but cannot fully assume the ternary state conformation until the DNA moves to the ternary position. The movements of Arg^{514} and Arg^{517} trigger flips of Ile^{492}, Phe^{506}, and Tyr^{505} in succession, and thus DNA motion toward the ternary state, after which Arg^{514} and Arg^{517} fully transition to positions in the ternary state.

CONCLUSION

The sequence of events presented here for pol λ emphasizes the main conclusion of this study that a delicate series of residue side-chain transitions assemble the active site for the nucleotidyl transfer reaction. Disruption of these side-chain rearrangements has extreme effects on the organization of the active site, as revealed by our mutation simulations. This result is paralleled by changes in enzyme efficiency, fidelity, and nucleotide binding described from experimental mutation studies of pol λ. Thumb subdomain motion, while traditionally considered to make a major contribution to the fidelity of an enzyme, may take a secondary role in the catalytic cycle of pol λ and stimulate or facilitate the assembly of the active site which is largely performed by residue side-chain adjustments and repositioning of the DNA. These residue side chains act as gate-keepers in orchestrating the evolution of the enzyme-substrate complex toward the chemical reaction. How these residue side chains select against incorrect nucleotides to monitor the fidelity of the enzyme will be a topic of future studies.

APPENDIX: GEOMETRIC CHARACTERISTICS

The movement of enzymes such as pol λ is not always accurately represented by a RMSD measure due to the magnitude and direction of domain motions. A previously developed scheme to represent the RMSD data more accurately in such situations was used to capture the motion of the DNA and subdomains in our pol-λ simulations (25). In this alternative approach, we project the RMSD of the simulated structure on the line joining the geometric centers of the structure in the crystal open and closed conformations. As shown in Fig. S5, this can be represented by a triangle where the crystal open and closed conformations form two vertices of the triangle and the simulated structure forms the third. The lengths of sides a and b of the triangle are given by the RMSD of the simulated structure relative to the crystal open conformation and crystal closed conformation, respectively, when the simulated structure and the corresponding crystal structure are superimposed with respect to all protein C_α atoms. The RMSD between the crystal open and closed conformations forms side c of the triangle and is held fixed. The shift distance, h, describes the displacement of

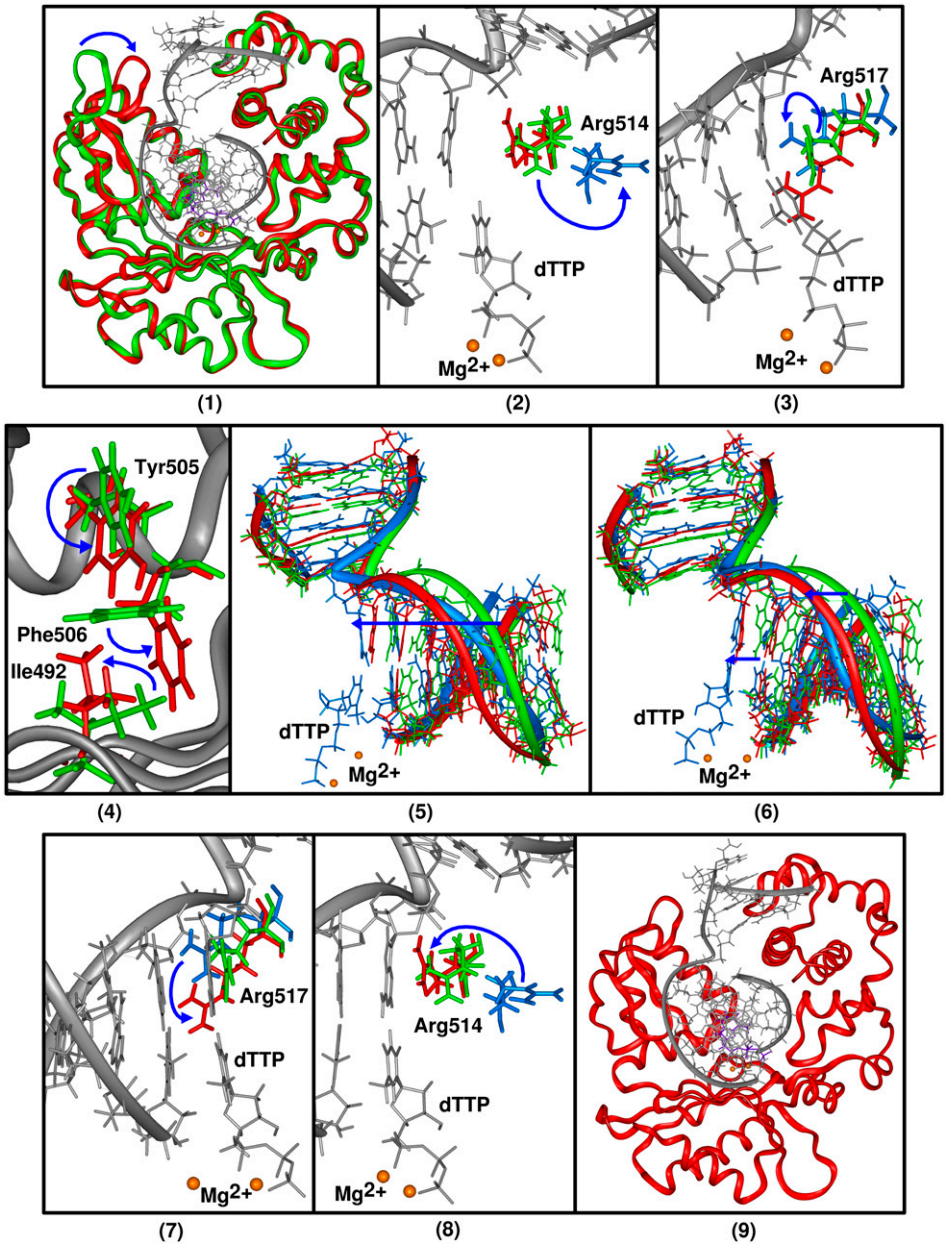

FIGURE 6 Proposed sequence of events for the catalytic cycle of DNA pol λ. In all panels, the x-ray crystal binary (PDB entry 1XSL) and ternary (PDB entry 1XSN) complexes are green and red, respectively, and intermediate conformations of residues and DNA are blue. Blue arrows represent motion. The correct incoming nucleotide, here dTTP, is shown in all panels with both the catalytic and nucleotide-binding ions (*gold spheres*) except panel 4. Panel 1 depicts the closing motion of the loop containing β-strand 8 in the thumb subdomain in response to binding of the correct incoming nucleotide, dTTP (*purple*); superimposed C_α traces of x-ray crystal binary and ternary are shown. Panel 2 shows the start of Arg^{514}'s transition from the binary to the ternary position with the flip of Arg^{514} from the binary state position away from the DNA as indicated by the arrow. Panel 3 shows the partial flip of Arg^{517} from the binary to the ternary position. Panel 4 shows the flips of Ile^{492}, Tyr^{505}, and Phe^{506} from the binary to the ternary state positions. Panel 5 shows the DNA in transition from the binary to the ternary state which occurs after the flips of Ile^{492}, Tyr^{505}, and Phe^{506}. Panel 6 shows the completed transition of the DNA to its ternary position. Panel 7 shows the completed flip of Arg^{517} from its intermediate position to the ternary position. Panel 8 shows the completed flip of Arg^{514} from its intermediate position to its ternary position. Panel 9 shows the closed active conformation of the pol λ/DNA complex with substrate (*purple*) and ions (*gold spheres*) bound.

the simulated structure in the direction perpendicular to the line joining the geometric centers of the structure in the crystal open and closed conformations. When h is constant, RMSD alone is a good measure of domain motions. When h is not constant, this is an appropriate method to use to represent domain motion toward the crystal states. The variable lengths L1 and L2 correspond to the projected RMSD of the simulated structure with respect to the crystal open and closed conformations, respectively.

SUPPLEMENTARY MATERIAL

An online supplement to this article can be found by visiting BJ Online at http://www.biophysj.org.

We thank S. Yaghmour for earlier contributions made to our research of pol λ. Molecular images were generated using VMD (62) and the INSIGHTII package (Accelrys, San Diego, CA).

This work was supported by National Science Foundation grant No. MCB-0316771, National Institutes of Health grant No. R01 ES012692, and the American Chemical Society Petroleum Research Fund (PRF award No. 39115-AC4) to T. Schlick. The work is made possible by support for the Xeon computer cluster by the National Center for Supercomputing Applications under grant No. MCA99S021, and for use of the NYU Chemistry Department supercomputer under grant No. CHE-0420870. M. Foley is supported by the National Science Foundation's IGERT program in Computational Biology at New York University.

REFERENCES

1. Garcia-Diaz, M., K. Bebenek, G. Gao, L. C. Pedersen, R. E. London, and T. A. Kunkel. 2005. Structure-function studies of DNA polymerase λ. *DNA Repair* (*Amst.*). 4:1358–1367.

2. Garcia-Diaz, M., K. Bebenek, R. Sabariegos, O. Dominguez, J. Rodriguez, T. Kirchhoff, E. Garcia-Palomero, A. J. Picher, R. Juarez, J. F. Ruiz, T. A. Kunkel, and L. Blanco. 2002. DNA polymerase λ, a novel DNA repair enzyme in human cells. *J. Biol. Chem.* 277:13184–13191.

3. Bebenek, K., M. Garcia-Diaz, L. Blanco, and T. A. Kunkel. 2003. The frameshift infidelity of human DNA polymerase λ. *J. Biol. Chem.* 278: 34685–34690.

4. Fiala, K. A., W. W. Duym, J. Zhang, and Z. Suo. 2006. Up-regulation of the fidelity of human DNA polymerase λ by its non-enzymatic proline-rich domain. *J. Biol. Chem.* 281:19038–19044.

5. Steitz, T. A. 1999. DNA polymerases: structural diversity and common mechanisms. *J. Biol. Chem.* 274:17395–17398.

6. Callebaut, I., and J. Mornon. 1997. From BRCA1 to RAP1: a widespread BRCT module closely associated with DNA repair. *FEBS Lett.* 400:25–30.

7. Bork, P., K. Hofmann, P. Bucher, A. F. Neuwald, S. F. Altschul, and E. V. Koonin. 1997. A superfamily of conserved domains in DNA damage-responsive cell cycle checkpoint proteins. *FASEB J.* 11:68–76.

8. Garcia-Diaz, M., K. Bebenek, T. A. Kunkel, and L. Blanco. 2001. Identification of an intrinsic 5′-deoxyribose-5-phosphate lyase activity in human DNA polymerase λ. *J. Biol. Chem.* 276:34659–34663.

9. Ahn, J., B. G. Werneburg, and M.-D. Tsai. 1997. DNA polymerase β: Structure-fidelity relationship from pre-steady-state kinetic analyses of all possible correct and incorrect base pairs for wild type and R283A mutant. *Biochemistry.* 36:1100–1107.

10. Ahn, J., V. S. Kraynov, X. Zhong, B. G. Werneburg, and M.-D. Tsai. 1998. DNA polymerase β: effects of gapped DNA substrates on dNTP specificity, fidelity, processivity and conformational changes. *Biochem. J.* 331:79–87.

11. Vande Berg, B. J., W. A. Beard, and S. H. Wilson. 2001. DNA structure and aspartate 276 influence nucleotide binding to human DNA polymerase β. *J. Biol. Chem.* 276:3408–3416.

12. Shah, A. M., S. X. Li, K. S. Anderson, and J. B. Sweasy. 2001. Y265H mutator mutant of DNA polymerase β. Proper teometric alignment is critical for fidelity. *J. Biol. Chem.* 276:10824–10831.

13. Suo, Z., and K. A. Johnson. 1998. Selective inhibition of HIV-1 reverse transcriptase by an antiviral inhibitor, (*R*)-9-(2-phosphonylmethoxypropyl)adenine. *J. Biol. Chem.* 273:27250–27258.

14. Kraynov, V. S., B. G. Werneburg, X. Zhong, H. Lee, J. Ahn, and M.-D. Tsai. 1997. DNA polymerase β: analysis of the contributions of tyrosine-271 and asparagine-279 to substrate specificity and fidelity of DNA replication by pre-steady-state kinetics. *Biochem. J.* 323:103–111.

15. Zhong, X., S. S. Patel, B. G. Werneburg, and M.-D. Tsai. 1997. DNA polymerase β: multiple conformational changes in the mechanism of catalysis. *Biochemistry.* 36:11891–11900.

16. Dahlberg, M. E., and S. J. Benkovic. 1991. Kinetic mechanism of DNA polymerase I (Klenow fragment): identification of a second conformational change and evaluation of the internal equilibrium constant. *Biochemistry.* 30:4835–4843.

17. Kuchta, R. D., V. Mizrahi, P. A. Benkovic, K. A. Johnson, and S. J. Benkovic. 1987. Kinetic mechanism of DNA polymerase I (Klenow). *Biochemistry.* 26:8410–8417.

18. Wong, I., S. S. Patel, and K. A. Johnson. 1991. An induced-fit kinetic mechanism for DNA replication fidelity: direct measurement by single-turnover kinetics. *Biochemistry.* 30:526–537.

19. Patel, S. S., I. Wong, and K. A. Johnson. 1991. Pre-steady-state kinetic analysis of processive DNA replication inducing complete characterization of an exonuclease-deficient mutant. *Biochemistry.* 30: 511–525.

20. Frey, M. W., L. C. Sowers, D. P. Millar, and S. J. Benkovic. 1995. The nucleotide analog 2-aminopurine as a spectroscopic probe of nucleotide incorporation by the Klenow fragment of *Escherichia coli* polymerase I and bacteriophage T4 DNA polymerase. *Biochemistry.* 34:9185–9192.

21. Capson, T. L., J. A. Peliska, B. F. Kaboord, M. W. Frey, C. Lively, M. Dahlberg, and S. J. Benkovic. 1992. Kinetic characterization of the polymerase and exonuclease activities of the gene 43 protein of bacteriophage T4. *Biochemistry.* 31:10984–10994.

22. Beard, W. A., D. D. Shock, X.-P. Yang, S. F. DeLauder, and S. H. Wilson. 2002. Loss of DNA polymerase β stacking interactions with templating purines, but not pyrimidines, alters catalytic efficiency and fidelity. *J. Biol. Chem.* 277:8235–8242.

23. Beard, W. A., D. D. Shock, and S. H. Wilson. 2004. Influence of DNA structure on DNA polymerase β active site function: extension of mutagenic DNA intermediates. *J. Biol. Chem.* 279:31921–31929.

24. Yang, L., W. A. Beard, S. H. Wilson, S. Broyde, and T. Schlick. 2002. Polymerase β simulations suggest that Arg^{258} rotation is a slow step rather than large subdomain motions *per se*. *J. Mol. Biol.* 317: 651–671.

25. Arora, K., and T. Schlick. 2004. In silico evidence for DNA polymerase β's substrate-induced conformational change. *Biophys. J.* 87: 3088–3099.

26. Arora, K., and T. Schlick. 2005. Conformational transition pathway of polymerase β/DNA upon binding correct incoming substrate. *J. Phys. Chem. B.* 109:5358–5367.

27. Arora, K., W. A. Beard, S. H. Wilson, and T. Schlick. 2005. Mismatch-induced conformational distortions in polymerase β support an induced-fit mechanism for fidelity. *Biochemistry.* 44:13328–13341.

28. Radhakrishnan, R., and T. Schlick. 2004. Orchestration of cooperative events in DNA synthesis and repair mechanism unraveled by transition path sampling of DNA polymerase β's closing. *Proc. Natl. Acad. Sci. USA.* 101:5970–5975.

29. Kunkel, T. A. 2004. DNA replication fidelity. *J. Biol. Chem.* 279: 16895–16898.

30. Showalter, A. K., B. J. Lamarche, M. Bakhtina, M.-I. Su, K.-H. Tang, and M.-D. Tsai. 2006. Mechanistic comparison of high-fidelity and error-prone DNA polymerases and ligases involved in DNA repair. *Chem. Rev.* 106:340–360.

31. Sawaya, M. R., R. Prasad, S. H. Wilson, J. Kraut, and H. Pelletier. 1997. Crystal structures of human DNA polymerase β complexed with gapped and nicked DNA: evidence for an induced fit mechanism. *Biochemistry.* 36:11205–11215.

32. Garcia-Diaz, M., K. Bebenek, J. M. Krahn, T. A. Kunkel, and L. C. Pedersen. 2005. A closed conformation for the pol λ catalytic cycle. *Nat. Struct. Mol. Biol.* 12:97–98.

33. Garcia-Diaz, M., K. Bebenek, J. M. Krahn, L. Blanco, T. A. Kunkel, and L. C. Pedersen. 2004. A structural solution for the DNA polymerase λ-dependent repair of DNA gaps with minimal homology. *Mol. Cell.* 13:561–572.

34. Delarue, M., J. B. Boulé, J. Lescar, N. Expert-Bezançon, N. Jourdan, N. Sukumar, F. Rougeon, and C. Papanicolaou. 2002. Crystal structures of a template-independent DNA polymerase: murine terminal deoxynucleotidyltransferase. *EMBO J.* 21:427–439.

35. Yang, L., W. A. Beard, S. H. Wilson, S. Broyde, and T. Schlick. 2004. Highly organized but pliant active site of DNA polymerase β: compensatory mechanisms in mutant enzymes revealed by dynamics simulations and energy analyses. *Biophys. J.* 86:3392–3408.

36. Steitz, T. A. 1998. A mechanism for all polymerases. *Nature.* 391: 231–232.

37. Brooks, B. R., R. E. Bruccoleri, B. D. Olafson, D. J. States, S. Swaminathan, and M. Karplus. 1983. CHARMM: a program for macromolecular energy, minimization, and dynamics calculations. *J. Comput. Chem.* 4:187–217.

38. Stote, R. H., and M. Karplus. 1995. Zinc binding in proteins and solution: a simple but accurate nonbonded representation. *Proteins.* 23:12–31.

39. MacKerell, A. D., Jr. 1997. Influence of magnesium ions on duplex DNA structural, dynamic and solvation properties. *J. Phys. Chem. B.* 101:646–650.

40. Yang, L., K. Arora, W. A. Beard, S. H. Wilson, and T. Schlick. 2004. The critical role of magnesium ions in DNA polymerase β's closing and active site assembly. *J. Am. Chem. Soc.* 126:8441–8453.

41. Qian, X., D. Strahs, and T. Schlick. 2001. A new program for optimizing periodic boundary models of solvated biomolecules (PBCAID). *J. Comput. Chem.* 22:1843–1850.

42. Klapper, I., R. Hagstrom, R. Fine, K. Sharp, and B. Honig. 1986. Focusing of electric fields in the active site of Cu-Zn superoxide dismutase: effects of ion strength and amino-acid modification. *Proteins.* 1:47–59.

43. MacKerell, A., Jr., and N. K. Banavali. 2000. All-atom empirical force field for nucleic acids. II. Application to molecular dynamics simulations of DNA and RNA in solution. *J. Comput. Chem.* 21:105–120.

44. Phillips, J. C., R. Braun, W. Wang, J. Gumbart, E. Tajkhorshid, E. Villa, C. Chipot, R. D. Skeel, L. Kale, and K. Schulten. 2005. Scalable molecular dynamics with NAMD. *J. Comput. Chem.* 26:1781–1802.

45. Feller, S. E., Y. Zhang, R. W. Pastor, and B. R. Brooks. 1995. Constant pressure molecular dynamics simulation: the Langevin piston method. *J. Chem. Phys.* 103:4613–4621.

46. Ryckaert, J.-P., G. Ciccotti, and H. J. C. Berendsen. 1977. Numerical integration of the Cartesian equations of motion of a system with constraints: molecular dynamics of *n*-alkanes. *J. Comput. Phys.* 23: 327–341.

47. Darden, T. A., D. M. York, and L. G. Pedersen. 1993. Particle mesh Ewald: an $N*log(N)$ method for Ewald sums in large systems. *J. Chem. Phys.* 98:10089–10092.

48. Wang, Y., K. Arora, and T. Schlick. 2006. Subtle but variable conformational rearrangements in the replication cycle of *Sulfolobus solfataricus* P2 DNA polymerase IV (Dpo4) may accommodate lesion bypass. *Protein Sci.* 15:135–151.

49. Osheroff, W. P., W. A. Beard, S. H. Wilson, and T. A. Kunkel. 1999. Base substitution specificity of DNA polymerase β depends on interactions in the DNA minor groove. *J. Biol. Chem.* 274:20749–20752.

50. Beard, W. A., W. P. Osheroff, R. Prasad, M. R. Sawaya, M. Jaju, T. G. Wood, J. Kraut, T. A. Kunkel, and S. H. Wilson. 1996. Enzyme-DNA interactions required for efficient nucleotide incorporation and discrimination in human DNA polymerase β. *J. Biol. Chem.* 271:12141–12144.

51. Beard, W. A., D. D. Shock, B. J. Vande Berg, and S. H. Wilson. 2002. Efficiency of correct nucleotide insertion governs DNA polymerase fidelity. *J. Biol. Chem.* 277:47393–47398.

52. Batra, V. K., W. A. Beard, D. D. Shock, J. M. Krahn, L. C. Pedersen, and S. H. Wilson. 2006. Magnesium-induced assembly of a complete DNA polymerase catalytic complex. *Structure.* 14:757–766.

53. Werneburg, B. G., J. Ahn, X. Zhong, R. J. Hondal, V. S. Kraynov, and M.-D. Tsai. 1996. DNA polymerase β: pre-steady-state kinetic analysis and roles of arginine-283 in catalysis and fidelity. *Biochemistry.* 35: 7041–7050.

54. Sampoli Benítez, B., K. Arora, and T. Schlick. 2006. In silico studies of the African swine fever virus DNA polymerase X support an induced-fit mechanism. *Biophys. J.* 90:42–56.

55. Radhakrishnan, R., and T. Schlick. 2005. Fidelity discrimination in DNA polymerase β: differing closing profiles for a mismatched (G:A) versus matched (G:C) base pair. *J. Am. Chem. Soc.* 127:13245–13252.

56. Radhakrishnan, R., K. Arora, Y. Wang, W. A. Beard, S. H. Wilson, and T. Schlick. 2006. Regulation of DNA repair fidelity by molecular checkpoints: ''Gates'' in DNA polymerase β's substrate selection. *Biochemistry.* (Accepted with revisions)

57. Beard, W. A., and S. H. Wilson. 2006. Structure and mechanism of DNA polymerase β. *Chem. Rev.* 106:361–382.

58. Shevelev, I., G. Blanca, G. Villani, K. Ramadan, S. Spadari, U. Hubscher, and G. Maga. 2003. Mutagenesis of human DNA polymerase λ: essential roles of Tyr^{505} and Phe^{506} for both DNA polymerase and terminal transferase activities. *Nucleic Acids Res.* 31:6916–6925.

59. Li, S. X., J. A. Vaccaro, and J. B. Sweasy. 1999. Involvement of phenylalanine 272 of DNA polymerase β in discriminating between correct and incorrect deoxynucleoside triphosphates. *Biochemistry.* 38: 4800–4808.

60. Crespan, E., S. Zanoli, A. Khandazhinskaya, I. Shevelev, M. Jasko, L. Alexandrova, M. Kukhanova, G. Blanca, G. Villani, U. Hubscher, S. Spadari, and G. Maga. 2005. Incorporation of non-nucleoside triphosphate analogues opposite to an abasic site by human DNA polymerases β and λ. *Nucleic Acids Res.* 33:4117–4127.

61. Osheroff, W. P., W. A. Beard, S. Yin, S. H. Wilson, and T. A. Kunkel. 2000. Minor groove interactions at the DNA polymerase β active site modulate single-base deletion error rates. *J. Biol. Chem.* 275:28033–28038.

62. Humphrey, W., A. Dalke, and K. Schulten. 1996. VMD—visual molecular dynamics. *J. Mol. Graph.* 14:33–38.